Development of Cationic Cellulose-Modified Bentonite−Alginate Nanocomposite Gels for Sustained Release of Alachlor

Xiaocheng Wang, Xiaojun Hou, Peiyu Zou, Min Zhang, and Lin Ma*

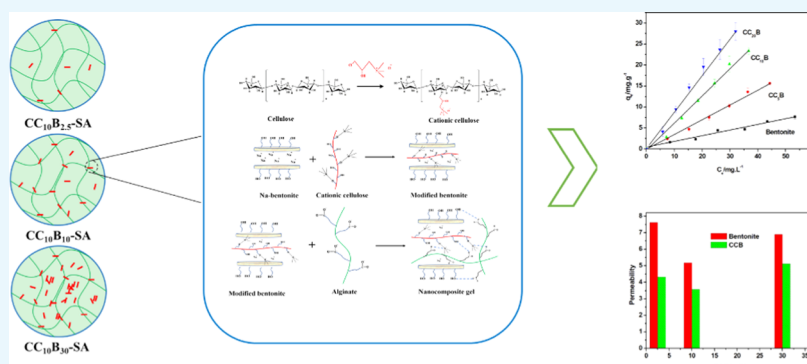Cite This: *ACS Omega* 2022, 7, 20032−20043

Read Online

ACCESS | Metrics & More | Article Recommendations | Supporting Information

ABSTRACT: The nanocomposite gel prepared from nanoclay and natural polysaccharides showed a good sustained-release property. Herein, a cationic cellulose-modified bentonite−alginate nanocomposite gel was prepared and used to enhance the sustained release of alachlor. The underlying effect and mechanism of the structure of modified bentonite−alginate nanocomposite gels on the release behavior of alachlor were explored by Fourier transform infrared (FTIR) spectroscopy, X-ray diffraction (XRD), scanning electron microscopy (SEM), and thermogravimetric (TG) analysis. The results showed that the release of alachlor from the nanocomposite gels was dominated by Fickian diffusion and closely related to the adsorption capacity and permeability of the matrix. The cationic cellulose intercalated into the interlayer space of bentonite through an ion exchange reaction, which significantly enhanced the hydrophobicity of bentonite and its interaction with alachlor. The stacking aggregation of bentonite nanoplatelets and permeability of the gel network were decreased through the electrostatic interaction between cationic cellulose and alginate molecular chains, thus remarkably enhancing the sustained-release property of the nanocomposite gel. The release kinetics revealed that the release rate of alachlor from the nanocomposite gel first decreased and then increased as the content of bentonite and modified bentonite gradually increased. Also, the best sustained-release property of the nanocomposite gel was obtained at bentonite and modified bentonite additions of about 10%, under which the release time of 50% alachlor (T_{50}) from bentonite−alginate and modified bentonite−alginate nanocomposite gels was 4.4 and 5.6 times longer than the release time from pure alginate gels, respectively.

1. INTRODUCTION

The widespread use of pesticides has greatly increased the production of agricultural products and largely met the demand for food from a continuously growing population.[1−3] However, the problems of wasting resources and environmental pollution caused by the misuse of pesticides are increasingly serious. Sustained-release formulations (SRFs), with outstanding features of extended shelf life, reduced frequency of use, reduced dosage and toxicity, enable more rational use of pesticides, and are also of greater importance to environmental protection.[4−6] Natural polysaccharide hydrogels are polymeric networks of natural polysaccharides (e.g., chitosan, cellulose, and alginate) cross-linked together, which are considered to be promising sustained-release carriers for drugs by virtue of their superior biocompatibility, high biodegradability, and low toxicity.[7−9] Unfortunately, the

practical application of natural polysaccharide hydrogel-drug carriers was limited owing to the poor mechanical properties, high water absorbency, and poor sustained-release properties.[10,11] The mechanical strength and sustained-release properties of natural polysaccharide hydrogels can be effectively enhanced by constructing interpenetrating (semi-interpenetrating) networks and adding nanofillers.[12−14]

The development and application of nanomaterials is an important development direction for current pesticide sustained-release technology.[4] Nanocomposites prepared from nanomaterials (e.g., ZnO, CuO, TiO$_2$, Ag) and polymers can not only take advantage of the inherent properties of both materials but also modulate the structure of the materials at the nanoscale, which has been widely used in the preparation of pesticide sustained-release formulations.[15,16] Nevertheless, the disadvantages of traditional nanomaterials such as the limitations of scale production, high cost, and environmental hazards should not be ignored. Consequently, nanoclay materials, represented by bentonite, gradually captured the attention of researchers.[17−19] Bentonite is a nonmetallic clay with montmorillonite as the main mineral component featuring a natural nanostructure, low cost, nontoxicity, and easy formation of nanoplatelets after full dispersion in water on account of the strong hydration of interlayer cations. It has wide applications in the preparation of nanocomposite gel delivery systems to obtain better mechanical properties, thermal stability, drug entrapment efficiency, and sustained-release properties.[20−22]

Alginate (SA) is a natural macromolecule polysaccharide composed of D-mannose and L-guronic acid units, which is easy to cross-link by divalent metal ions such as Ca^{2+} and Mg^{2+} and is one of the most widely used substrates for sustained-release drug carriers.[23,24] Previous work had shown that the sustained-release property of the alginate gel could be enhanced by adding a small amount of bentonite. However, the sustained-release property of the nanocomposite gel rather weakened at a high content (>10%) of bentonite.[25] An identical result was obtained in the release of diclofenac sodium from bentonite−urealilpoly(ethylene oxide) (UPEO) composite gels.[26] In addition, further studies showed that excessive bentonite nanoplatelets were hardly able to form stable bonds through hydrogen bonding between hydroxyl groups on the surface and alginate molecules and tended to stack and form a large number of micropores in the nanocomposite gel, which eventually resulted in a decrease in the sustained-release property of the nanocomposite gel.[25] Therefore, the sustained-release property of bentonite−polymer nanocomposite gels could be further improved by enhancing the interaction between bentonite and macromolecules and promoting the adequate dispersion of bentonite nanoplatelets in the polymer matrix. The organic modification of bentonite can meet these conditions very well.

It is an important method to adjust the surface properties of bentonite nanoplatelets via the modification of bentonite using cationic polymers.[27] In contrast to small organic cations such as alkyl quaternary ammonium salts, cationic polymers can not only modify the surface of bentonite but also form interpenetrating networks with alginate, which may enhance the sustained-release properties of nanocomposite gels. Cellulose is a branched polysaccharide composed of glucose and is the most abundant polymer in biomass, which features low production cost, good biodegradability, and excellent biocompatibility.[28,29] Cellulose is easy to be esterified, penalized, and etherified because of its rich hydroxyl groups. Therefore, cationic cellulose (CC) can be obtained by the reaction of cellulose with (3-chloro-2-hydroxypropyl)trimethylammonium chloride (CHPTMAC).[30,31] By far, most studies on cationic cellulose have focused on cosmetics, paper additives, and antibacterial agents;[32] surprisingly, little attention has been paid to using cationic cellulose to adjust the surface property of

bentonite and constructing interpenetrating (semi-interpenetrating) networks.

Here, cationic cellulose was prepared by modifying cellulose with (3-chloro-2-hydroxypropyl)trimethylammonium chloride and used as a modifier for bentonite. The isothermal adsorption of alachlor on cationic cellulose-modified bentonite was studied, and the interaction between alachlor and modified bentonite was also analyzed. Thereafter, the cationic cellulose-modified bentonite−alginate nanocomposite gel was used as the substrate to prepare the sustained-release particles of alachlor and the effect and mechanism of the structure of nanocomposite gels on release behavior of alachlor were analyzed more deeply by Fourier transform infrared (FTIR) spectroscopy, X-ray diffraction (XRD), scanning electron microscopy (SEM), and thermogravimetric (TG) analysis. It lays a foundation for the regulation of the sustained-release property of nanocomposites based on bentonite and natural polymers and their development and application in pesticide sustained-release formulations and is of great significance for environmental protection.

2. MATERIALS AND METHODS

2.1. Materials. Sodium alginate with a viscosity ≥2000 cps for a 2% solution at 25 °C was purchased from Sigma Co. Na-bentonite with a cation exchange capacity of 0.85 mmol·g^{-1} was purchased from Guangdong Wengjiang Chemical Reagent Co. Ltd. (China). Cellulose and (3-chloro-2-hydroxypropyl)-trimethylammonium chloride (CHPTMAC) were obtained from Shanghai Macklin Biochemical Technology Co., Ltd. (China). Disodium ethylenediamine tetraacetic acid (EDTA) was provided by Sinopharm Chemical Reagent Ltd. (China). Technical-grade alachlor (98%) was supplied by Guangxi Tianyuan Biochemical Ltd. (China). Chromatographic-grade methanol and analytical-grade ethanol were received from Shantou Xilong Chemical Reagent Ltd. The water used in the experiment is deionized.

2.2. Preparation of CC. The CC was prepared by referring to the previously reported method with some modifications.[33] Briefly, 2.0 g of cellulose was suspended in 20 mL of NaOH solution (pH = 11) in a 50 mL beaker containing 2.0 g of urea and stirred for 1 h at −10 °C. Then, the suspension was heated to −2 °C under agitation to dissolve the cellulose completely, and 4.0 g of CHPTMAC was added at 60 °C to keep the etherification reaction for 4 h. Afterward, the solution was poured into 300 mL of methanol, the obtained precipitates were separated by centrifugation (XiangYi L550, 3500 rpm), and the pH was adjusted to neutral with a 1:1 mixture of methanol/distilled water. Finally, the resulting product was freeze-dried and stored at 4 °C under hermetic conditions until further use.

2.3. Preparation of CCB. Briefly, 5.0 g of Na-bentonite was dispersed in 250 mL of deionized water in a 500 mL beaker at 60 °C followed by ultrasonication for 20 min. Subsequently, 0.25, 0.5, and 1.0 g of CC were added respectively to react for 4 h under agitation. The unreacted CC was removed by centrifugation three times. The resulting modified bentonite was dried to constant weight at 60 °C and labeled as CC$_x$B, whereas "x" is the mass percentage of cationic cellulose to bentonite including CC$_5$B, CC$_{10}$B, and CC$_{20}$B.

2.4. Adsorption Isotherms of Alachlor on CCB. Unmodified bentonite and modified bentonite (50 mg) were precisely weighed and placed in a conical flask containing 50 mL of alachlor solution (10−60 μg·mL^{-1}), respectively. The

mixture solution was stirred for 6 h in a thermostatic bath at 25 °C to reach the adsorption equilibrium (preliminary experiment indicated that adsorption equilibrium had reached this condition). Afterward, the samples were centrifuged at 10 000 rpm for 10 min, and the alachlor content of the supernatants was determined by HPLC. The isothermal adsorption of alachlor was calculated according to the concentration difference before and after adsorption. Under the same conditions, the results were measured in parallel three times, and the average value was taken.

2.5. Determination of Alachlor Content by HPLC. Solutions containing alachlor were passed through nylon filters of 0.22 μm pore diameter and then analyzed by HPLC (Shimadzu SPD-10A) equipped with a UV–vis detector set at 220 nm and a Hypersil ODS column (250 mm × 4.6 mm, 5 μm). The mobile phase was a methanol/water mixture (10:1) at a flow rate of 1.0 mL·min^{-1}.

2.6. Preparation of Nanocomposite Gel Particles and Films. About 0.1 g of alachlor was predissolved in 1 mL of methanol and slowly dropped in 50 mL of deionized water to form an emulsion. Then, different amounts of SA and CC$_{10}$B were added according to Table 3 and stirred for 4 h at room temperature to form a uniform suspension. Thereafter, the suspension was dropped in 0.5 M CaCl$_2$ solution by a syringe and allowed to cross-link for 15 min. Subsequently, the obtained nanocomposite gel particles were filtered and the residual CaCl$_2$ on the surface was removed using 300 mL of deionized water. Finally, the nanocomposite gel particles were dried to constant weight at 45 °C and labeled as A−CC$_x$B$_y$−SA. The gel particles without alachlor were prepared following the same procedure and labeled as CC$_x$B$_y$−SA, whereas "y" is the mass percentage of modified bentonite in the nanocomposite gel.

The nanocomposite gel films were prepared by solution casting. The modified bentonite−alginate and unmodified bentonite−alginate slurries were prepared according to the above method. The required slurry was accurately weighed and poured into polystyrene Petri dishes. Then, 0.5 M CaCl$_2$ solution was carefully added along the edge of the Petri dish. The cross-linking was allowed for 15 min and the obtained hydrogel films were dried at 45 °C.

The alachlor-loaded bentonite−alginate nanocomposite gel particles and films were also prepared according to the same method and labeled as A−B$_y$−SA, whereas "y" is the mass percentage of bentonite. The nanocomposite gel film was used for FTIR, XRD, and SEM analyses.

2.7. Determination of the Average Diameter of Nanocomposite Gel Particles. The average diameter of nanocomposite gel particles was measured by a Malvern Mastersizer 3000 dynamic scattering spectrometer (U.K., Malvern) using water as the medium.

2.8. FTIR Analysis. Cellulose, CC, bentonite, and CCB samples were mixed with KBr powers at a ratio of 2:100 by weight and then compressed to make a disk for FTIR characterization. The infrared spectrum was obtained using a Fourier transform infrared spectrometer (PerkinElmer) with KBr blank pressing as the background. The scanning range was 4000−400 cm^{-1} with a resolution of 4 cm^{-1}. The nanocomposite gel films were cut into 2 cm^2 squares, and the FTIR spectra were directly measured by the transmission method with air as the background.

2.9. XRD Analysis. XRD analyses of cellulose, CC, bentonite, CCB, and nanocomposite gel films were carried out using a Rigaku SmartLab3KW diffractometer (Japan) with Ni-filtered Cu Kα characteristic radiation (λ = 1.5405 Å). The scanning rate, scanning step, and scanning range were 10°· min^{-1}, 0.02, and 2−60°, respectively. The bentonite base spacing (d_{001}) was calculated by the Bragg equation ($2d \sin \theta$ = nλ).

2.10. SEM Analysis. The nanocomposite gel films were fixed on the metal column, and the surface was sprayed with gold. The apparent morphology was observed using a PHENOM F16502 scanning electron microscope (Holland, Phenom-World Feiner) at 5 kV and a working distance of 6.8 mm.

2.11. TG Analysis. Thermal properties of CC, bentonite, CCB, and nanocomposite gel particles were recorded on a NETZSCH STA 449 F3 thermal analysis instrument (German). The heating range was 25−400 °C at a heating rate of 10 °C·min^{-1} under nitrogen flow (100 mL·min^{-1}).

2.12. Analysis of Water Absorption Properties of Nanocomposite Gel Particles. About 0.4 g of nanocomposite gel particles was placed in a beaker containing 50 mL of deionized water at room temperature. The particles were removed at a preset time interval and the surface was dried with filter paper, and the water absorption and swelling rates of the gel particles were subsequently measured using the weighing method. Three parallel tests were carried out under the same conditions, and the results were taken as the average.

2.13. Analysis of the Alachlor Loading Rate. About 0.1 g of gel particles with alachlor were fully dispersed in 10 mL of EDTA solution (100 g·L^{-1}) under agitation to destroy the gel structure, and then, alachlor was extracted twice with 20 mL of methanol. The extract was centrifuged, and the supernatant was collected and fixed in a 50 mL volumetric flask. The content of alachlor in the solution was determined by HPLC to calculate the alachlor loading rate and the entrapment efficiency of the gel particles.

2.14. Release Kinetics of Alachlor. The nanocomposite gel particles with 4 mg of alachlor were added to 100 mL of deionized water (pH∼6.5) at a shaking rate of 150 r·min^{-1} at 25 °C. About 2 mL of supernatant was taken out at a preset time interval and replenished with 2 mL of deionized water. The supernatant was filtered and analyzed by HPLC to calculate the amount of the released alachlor, and then, the cumulative release profile of alachlor from nanocomposite gel particles was obtained.

3. RESULTS AND DISCUSSION

3.1. Preparation and Characterization of CC and CCB. CC and CCB were successfully prepared, and the organic carbon contents of cellulose and bentonite before and after modification were determined by elemental analysis (Table 1).

Table 1. Carbon Content f_{oc}, Basal Spacing d_{001}, and Equilibrium Constant K_a for Alachlor Adsorption on Cationic Cellulose-Modified Bentonites

sample	f_{oc} (%)	d_{001} (nm)	$K_a \times 10^{-3}$ (mL g^{-1})	R
cellulose	44.35			
cationic cellulose	45.12			
Na-bentonite	0.14	1.21	0.14	0.988
CC$_5$B	1.98	1.45	0.36	0.995
CC$_{10}$B	3.85	1.45	0.68	0.992
CC$_{20}$B	5.64	1.45	0.90	0.994
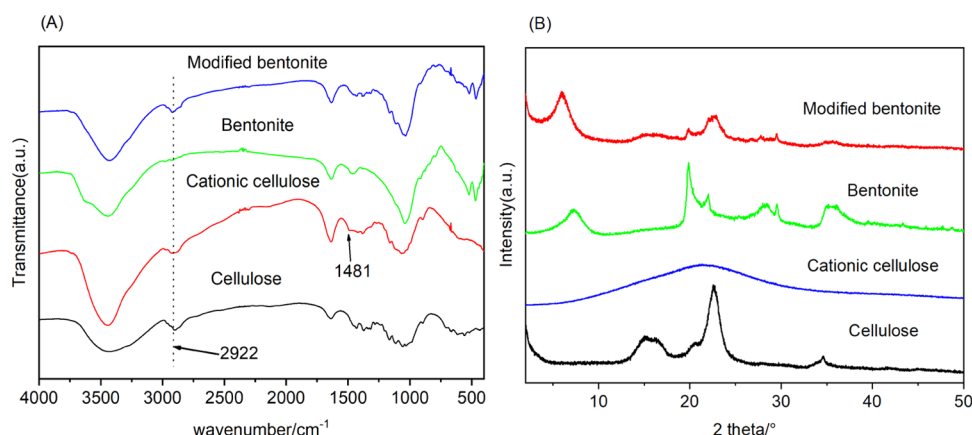
Figure 1. (A) FTIR spectra and (B) XRD patterns of cellulose, cationic cellulose, bentonite, and modified bentonite (CC_5B, $CC_{10}B$, $CC_{20}B$).

The carbon content of unmodified cellulose was 44.35%, which was very close to the theoretical value (44.44%). The carbon content of CC was 45.12%, and the corresponding grafting rate of CHPTMAC on the cellulose molecular chain was about 45.64%. The carbon content of Na-bentonite used in the experiment was almost negligible (0.14%). When the mass percentage of cationic cellulose was 5, 10, and 20%, the carbon content of CCB was 1.98, 3,85, and 5.64%, which corresponded to CC loadings of 87.77, 85.33, and 62.50%, respectively.

Infrared spectroscopy is an effective method for structural identification and qualitative analysis of materials. As shown in Figure 1A, the characteristic adsorption bands of cellulose at 3436 cm^{-1} resulted from the O−H bending, and the stretching vibration of the C−H appeared at 2898 cm^{-1}, while those at 1432, 1320, 1065, and 660 cm^{-1} could be ascribed to CH_2 bending, O−H bending, C−O stretching, and C−OH bending, respectively.[34] After being modified with CHPTMAC, the new absorption band of CC at 1481 cm^{-1} was attributed to the C−H stretching vibration of the methyl group on the quaternary ammonium group, suggesting that CC was successfully prepared.[35] In the FTIR spectra of Na-bentonite, the characteristic adsorption bands at 3434 cm^{-1} resulted from the O−H stretching and the O−H bending appeared at 1638 cm^{-1}. The bands at 1041 and 468 cm^{-1} were ascribed to the Si−O stretching and Si−O−Si bending vibrations, respectively.[36−38] After CC modification, CCB showed the new adsorption band at 2922cm^{-1}, which was assigned to the C−H stretching vibration in cationic cellulose, demonstrating that CC had been intercalated successfully into the interlayer space of bentonite.

The XRD patterns of bentonite, CC, and CCB (CC_5B, $CC_{10}B$, $CC_{20}B$) are shown in Figure 1B. The characteristic reflections of cellulose at 15.1, 16.4, and 22.6° corresponded to the ($1\bar{1}0$), (110), and (200) crystallographic planes.[39] After being grafted with CHPTMAC, CC showed a broad and weak (110) reflection at 21.26°, suggesting crystal transformation from cellulose I to cellulose II and that the hydrogen bonds between cellulose molecules were destroyed. Bentonite was a clay mineral with montmorillonite as the main component and had obvious (001) and (110) reflections at 2θ = 7.3 and 19.9°,[40] which corresponded to the bentonite spacing (d-value) of 1.21 nm. Bentonite often contains a small amount of clay impurities such as illite and kaolin and nonclay impurities such as quartzite and mica, and several weak reflections appeared in the range of 20−30°. After being modified with

CC, the reflection of the (001) plane of bentonite shifted toward a smaller reflection angle (2θ = 6.1°, d_{001} = 1.51 nm), indicating that CC was successfully intercalated into the interlayer space of bentonite and formed an electrostatic bond with the bentonite surface.

3.2. Adsorption Isotherms and Thermodynamics of Alachlor on CCB. To study the interaction between modified bentonite and alachlor, the adsorption isotherm of alachlor on CCB was determined (Figure 2). Within the concentration
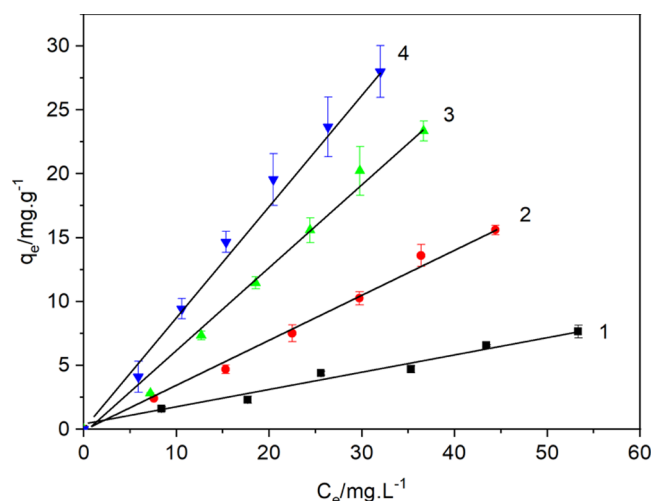

Figure 2. Isotherms for alachlor adsorption on cationic cellulose-modified bentonite: (1) bentonite, (2) CC_5B, (3) $CC_{10}B$, and (4) $CC_{20}B$.

range of the experimental study (10−60 μg·mL^{-1}), the adsorption capacity of alachlor on unmodified and modified bentonite increased linearly with increasing concentration of alachlor in solution. Therefore, the adsorption isotherm was linearly fitted, and the apparent adsorption constant (K_a) of alachlor was obtained from the slope. According to the K_a values in Table 1, the adsorption capacity of bentonite for alachlor was dramatically enhanced after CC modification, and the K_a values increased with the increase of CC content.

3.3. Preparation and Characterization of B−SA and CCB−SA Nanocomposite Gel Particles. The SA nanocomposite gel particles containing different contents of CCB (0−30%) were prepared successfully. A preliminary experiment indicated that $CC_{10}B$ displayed the highest efficiency to

Table 2. Formulation and characteristics of bentonite−alginate and modified bentonite−alginate nanocomposite gel with and without alachlor

| sample	alachlor/%	alginate/%	$CC_{10}B$/%	water/%	diameter/mm	content/mg·g^{-1}	encapsulation efficency/%
SA		2.00	0	98.0	1.54(0.01)		
$CC_{10}B_{2.5}$−SA		1.95	0.05	98.0	1.54(0.02)		
$CC_{10}B_5$−SA		1.90	0.10	98.0	1.51(0.02)		
$CC_{10}B_{10}$−SA		1.80	0.20	98.0	1.48(0.01)		
$CC_{10}B_{20}$−SA		1.60	0.40	98.0	1.48(0.03)		
$CC_{10}B_{30}$−SA		1.40	0.60	98.0	1.53(0.01)		
A−SA	0.20	2.00	0	97.8	1.56(0.01)	37.5	41.3
A−$CC_{10}B_{2.5}$−SA	0.20	1.95	0.05	97.8	1.56(0.03)	37.8	41.6
A−$CC_{10}B_5$−SA	0.20	1.90	0.10	97.8	1.54(0.01)	37.9	41.7
A−$CC_{10}B_{10}$−SA	0.20	1.80	0.20	97.8	1.50(0.02)	38.5	42.4
A−$CC_{10}B_{20}$−SA	0.20	1.60	0.40	97.8	1.52(0.02)	38.7	42.6
A−$CC_{10}B_{30}$−SA	0.20	1.40	0.60	97.8	1.55(0.01)	38.9	42.8
A−$B_{2.5}$−SA	0.20	1.95	0.05	97.8	1.52(0.01)	26.0	28.6
A−B_5−SA	0.20	1.90	0.10	97.8	1.49(0.04)	27.6	30.4
A−B_{10}−SA	0.20	1.80	0.20	97.8	1.51(0.02)	25.6	28.2
A−B_{20}−SA	0.20	1.60	0.40	97.8	1.46(0.03)	27.2	29.9
A−B_{30}−SA	0.20	1.40	0.60	97.8	1.40(0.02)	26.4	29.0
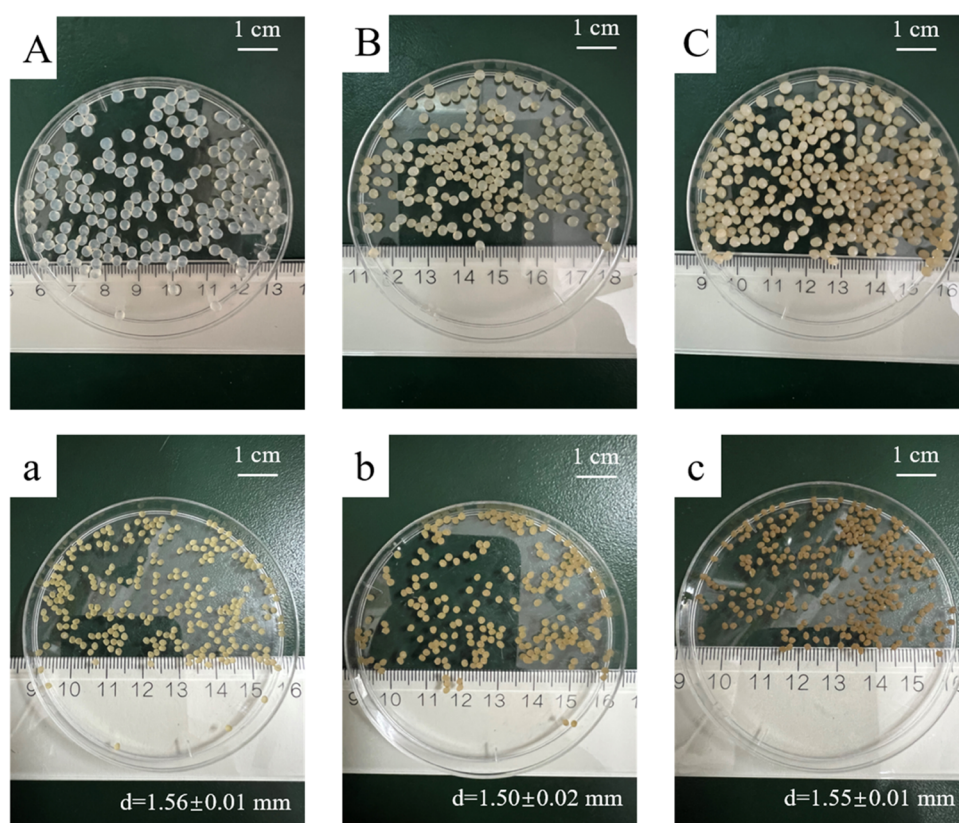
Figure 3. Typical photographs of alachlor-loaded alginate nanocomposite beads before (A−C) and after (a−c) drying: (A, a) A−SA, (B, b) A−$CC_{10}B_{10}$−SA, and (C, c) A−$CC_{10}B_{30}$−SA.

retard the release of alachlor from the nanocomposite (Figure S1). Thus, the nanocomposite with bentonite and $CC_{10}B$ of different amounts, with and without alachlor, are characterized in detail. The particle size and the content of alachlor of nanocomposite gel particles were determined and presented in Table 2. Typical photographs of the resulting gel particles before and after drying were shown in Figure 3. The CCB−SA nanocomposite gel particles were generally spherical with an average particle size of 1.48−1.54 mm after drying, while the loading of alachlor led to an increase in the size of the gel

particles with a particle size of 1.50−1.62 mm. Due to the high solubility in water (242 mg·L^{-1}), some of the alachlor was lost during the preparation of the sustained-release particles and the resulting alachlor loading in the SA gel particles was only 37.3 mg·g^{-1}, with a corresponding encapsulation rate of approximately 41.0%. The loading and encapsulation rate of alachlor in the nanocomposite gel particles slightly increased owing to the addition of CCB.

3.4. FTIR. To further explore the structure of the nanocomposite gels, the FTIR spectra of the gel films were

obtained and are summarized in Figure 4. The characteristic adsorption bands of SA at 3438, 1615, 1402, 949, and 883
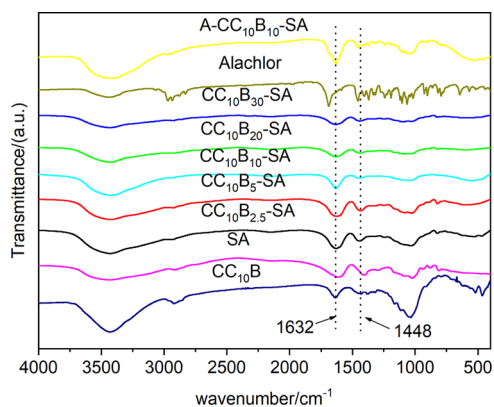
Figure 4. FTIR spectra of alginate, alachlor, and cationic cellulose-modified bentonite−alginate nanocomposites with and without alachlor.

cm^{-1} corresponded to the O−H vibration, symmetric and asymmetric stretching vibration of the carboxylate, C−O−C stretching vibration, and C−O stretching vibration, respectively.[41,42] The main infrared characteristic bands of CCB were similar to those of SA gels. After adding CCB, the symmetric and asymmetric stretching vibration of the carboxylate of SA showed a noticeable blue shift, suggesting that there might be electrostatic interactions between CCB and SA.[43]

As can be seen from Figure 4, the FTIR spectra of alachlor were very complicated. The new characteristic bands of alachlor-loaded nanocomposite gel appeared at 3100−2850 cm^{-1} (C−H stretching vibration of the benzene ring, methyl, and methylene), 1300−1000 cm^{-1} (C−H in-plane bending vibration of the benzene ring), and 710−650 cm^{-1} (C−H out-plane bending vibration of the benzene ring). The stretching vibration of the SA carboxyl group was significantly enhanced by superposition with the stretching vibration of the alachlor amide group C=O (1688 cm^{-1}), the C−H bending vibration of methyl and methylene (1450−1350 cm^{-1}), and the vibration absorption of the aromatic ring skeleton (1500−1400 cm^{-1}).

3.5. XRD. XRD patterns of A−B−SA and A−CCB−SA nanocomposite gel films are shown in Figure 5. As shown in Figure 5A, the diffraction pattern of pure SA gel showed weak reflection and no peaks indicative of crystalline phases in the

range of 2−50°, which suggested that the SA gel was mainly composed of amorphous structures.[44] The bentonite nano-platelets were easily stacked in alginate gel, and the weak reflection characteristics of bentonite such as the reflections of the (001) plane, (110) plane, and clay impurities could be observed in nanocomposite gels with a 5% bentonite addition. Also, the reflection intensity of the (001) plane increased rapidly with increasing bentonite addition, and the reflection angle gradually approached that of bentonite. In contrast, the addition of CCB had no obvious effect on the XRD reflection of SA gels (Figure 5B), and the weak reflection of the bentonite (001) plane was observed only when the addition of modified bentonite was at 30%, implying the good dispersion of modified bentonite nanoplatelets in the SA gel network via electrostatic interaction between surface-bound CC and SA.

3.6. SEM. The surface morphology of the carrier is an important parameter affecting drug release behavior. To reveal the effect of CCB on the apparent morphology of alginate gels, SEM was used to observe the apparent morphologies of A−B−SA and A−CC$_{10}$B−SA nanocomposite gel films. As shown in Figure S2, the pure SA gel film had a smooth and compact surface. In addition to a slight increase in surface roughness, the addition of bentonite had little influence on the surface integrity of the nanocomposites at a low loading level (<10%). However, the cracks on the surface of the gel film appeared as the mass percentage of bentonite further increased, and the number and size of which increased with an increase of bentonite content, indicating that SA was insufficient to accommodate the clay nanoplatelets. The aggregation of the clay nanoplatelets weakened the cross-linking within the polymeric network and destroyed the integrity of the matrix. In contrast, the addition of CCB had little influence on the apparent morphology of SA gels. When the mass percentage of CCB was about 20%, the stacking of bentonite occurred and the cracks appeared on the surface (Figure 6). However, the number and size of cracks were much smaller than those of A−B−SA. This suggested that the modification of CC significantly enhanced the interaction between bentonite nanoplatelets and SA chains and facilitated the structural integrity of gels, which was consistent with XRD analysis.

3.7. TG. TG and DTG curves of bentonite, CC, CCB, and CCB−SA nanocomposite gel particles are presented in Figure 7. Bentonite was an inorganic mineral and usually had good thermal stability, but the formation process of bentonite produced a permanent negative charge on the surface of the crystal layer due to the occurrence of holocrystalline
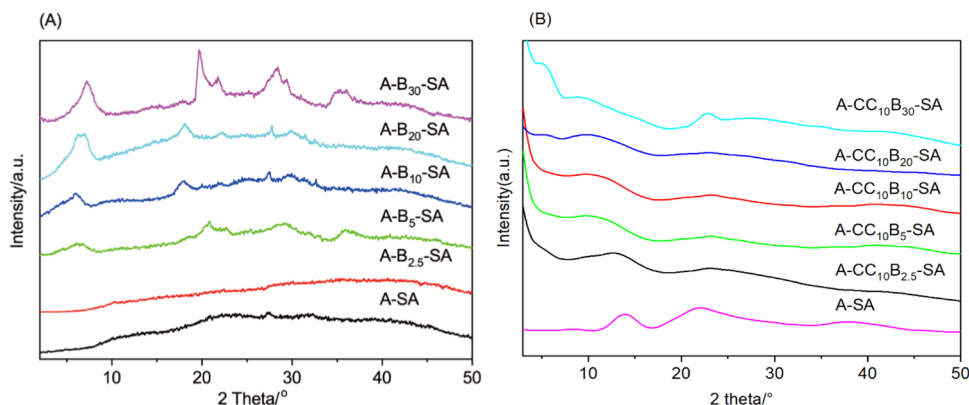
Figure 5. XRD patterns of alachlor-loaded alginate nanocomposites with unmodified bentonite (A) and cationic cellulose-modified bentonite (B).
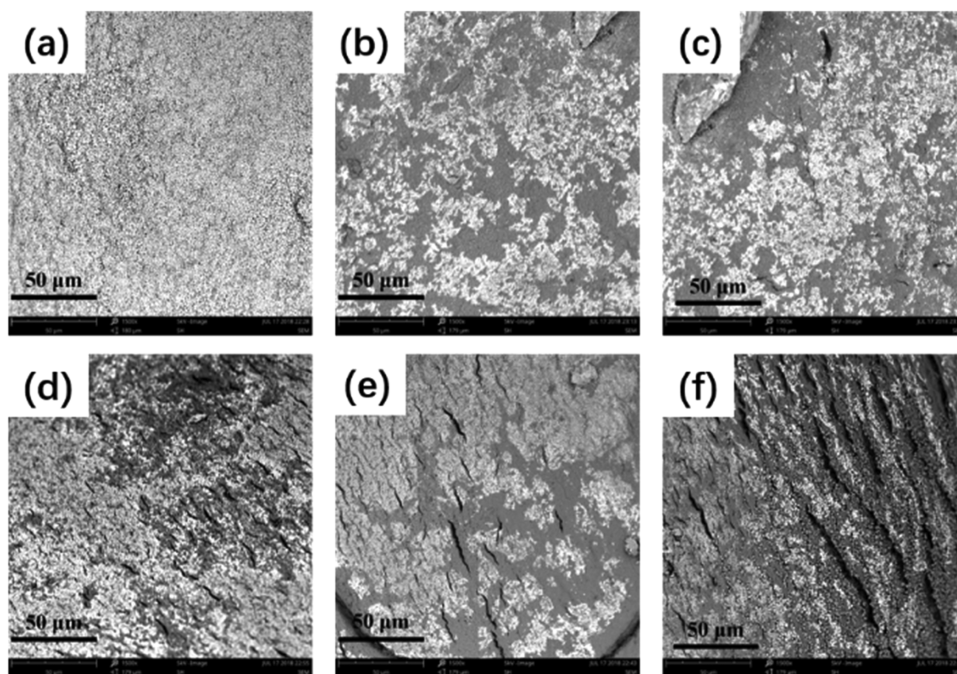
Figure 6. SEM images of alachlor-loaded alginate nanocomposites with cationic cellulose-modified bentonite: (a) A−SA, (b) A−CC$_{10}$B$_{2.5}$−SA, (c) A−CC$_{10}$B$_5$−SA, (d) A−CC$_{10}$B$_{10}$−SA, (e) A−CC$_{10}$B$_{20}$−SA, (f) A−CC$_{10}$B$_{30}$−SA.
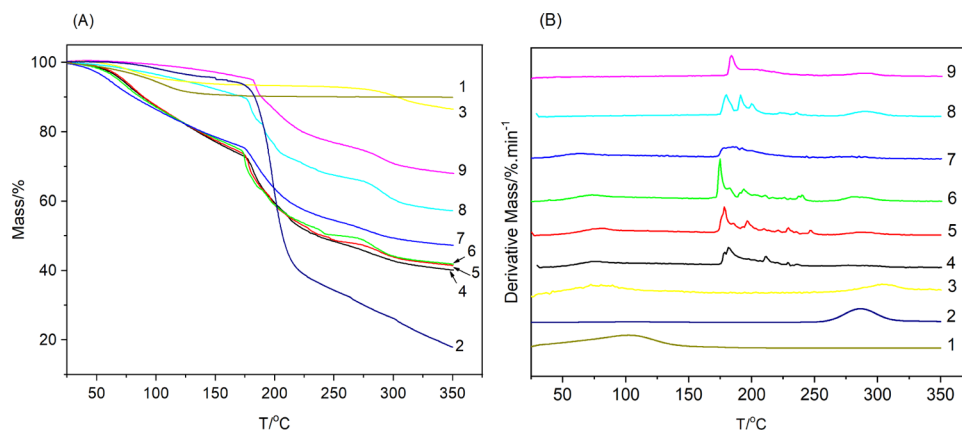

Figure 7. TG (A) and DTG (B) curves of alginate nanocomposite hydrogels with cationic cellulose-modified bentonite: (1) bentonite, (2) cationic cellulose, (3) CC$_{10}$B, (4) SA, (5) CC$_{10}$B$_{2.5}$−SA, (6) CC$_{10}$B$_5$−SA, (7) CC$_{10}$B$_{10}$−SA, (8) CC$_{10}$B$_{20}$−SA, and (9) CC$_{10}$B$_{30}$−SA.

substitution, and the interlayer binding of Na$^+$, K$^+$ and Ca^{2+} was highly hydrophilic. So, there was an obvious mass loss peak due to the removal of water molecules adsorbed between the layers of bentonite during heating.[45] The thermal decomposition process of polysaccharides was more complex, which involved the desorption of physically adsorbed water, the dehydration of structural hydroxyl, the fracture of C−O and C−C bonds in the glycoside chain, and the formation of coke.[46] As shown in Figure 7, there was a small mass loss peak of CC below 150 °C, which was due to the removal of adsorbed and bound water, and the dehydrated CC underwent pyrolysis from 171 °C, with the maximum mass loss rate occurring near 287 °C. The mass loss of CCB between 35 and 190 °C was caused by the removal of water molecules, while the mass loss peak between 225 and 350 °C should be attributed to the pyrolysis of CC bound to the bentonite nanoplatelets. Compared to the thermodynamic properties of cellulose in the literature,[47] CC showed lower thermal stability,

which was attributed to the decrystallinity of cellulose after quaternization and the thermal unstability of CHPTMAC.[48,49] A further comparison revealed that the CCB dehydration mass loss rate (7.3%) was between that of bentonite (9.9%) and CC (5.4%), whereas the maximum mass loss rate occurred at a lower temperature (79.4 °C) than those of bentonite (105 °C) and CC (98.2 °C), indicating that the affinity of the bentonite surface for water was significantly reduced on account of CC modification (Table S1). This indicated a good agreement with the enhanced adsorption of alachlor on CCB.

The SA gels also showed small mass loss due to dehydration when heated below 170 °C, and the rate of mass loss was much lower than that of the powder samples of bentonite, CC, and CCB, which may be due to the diffusion of water molecules being prevented by the alginate gel network. As the temperature increased, the SA gel began to pyrolyze and two distinct mass loss peaks appeared near 184 and 288 °C.[50] Inorganic minerals usually have better thermal stability, and
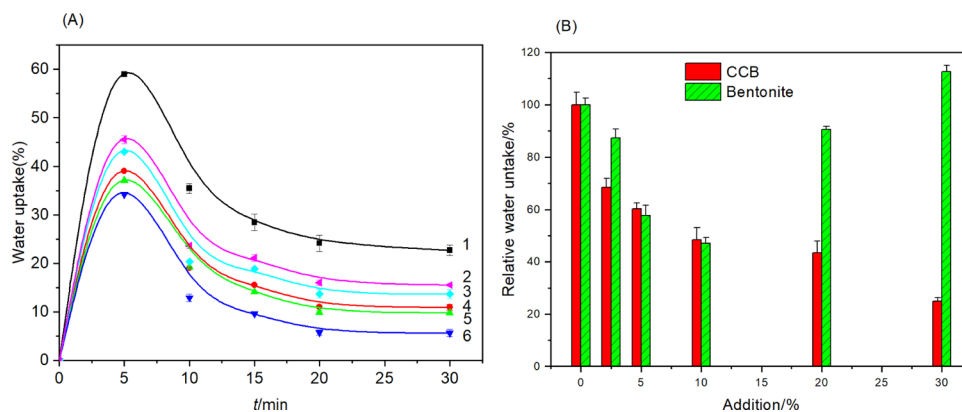
Figure 8. (A) Kinetics of water uptake of alginate nanocomposites with cationic cellulose-modified bentonite: (1) SA, (2) $CC_{10}B_{2.5}$–SA, (3) $CC_{10}B_5$–SA, (4) $CC_{10}B_{10}$–SA, (5) $CC_{10}B_{20}$–SA, and (6) $CC_{10}B_{30}$–SA. (B) Influence of addition of cationic cellulose-modified and unmodified bentonite on the saturated water uptake of alginate nanocomposites.

the addition of mineral clays often results in better thermal stability of polymers.[51,52] The temperature corresponding to the maximum mass loss rate of CCB combined with CCB pyrolysis (320 °C) was significantly higher than that of CC (288 °C). However, studies by Chang, Bharadwaj, and Amanda showed that the thermal stability of PLA, polyester, and starch was reduced due to the addition of bentonite, a phenomenon they attributed to the interaction of bentonite with polymers.[53−55] As can be seen from Figure 7, the decomposition temperature of SA particles decreased due to the addition of a small amount (<20%) of CCB, opposite to the behavior of the gel with higher CCB loading, which was similar to the results of the thermogravimetric analysis of the bentonite−alginate composite gel.[25] Further comparison revealed that CCB was more effective in reducing the thermal stability of SA, and the addition of 10% CCB reduced the maximum mass loss temperature of the SA gel by about 11 °C (from 185 to 174 °C) under optimal release conditions. In contrast, the addition of 10% bentonite only reduced the maximum mass loss temperature of the SA gel by about 3 °C (from 188 to 185 °C), indicating that the SA molecular chains in the composite gel formed a closer contact with the bentonite through electrostatic interactions with CC.

3.8. Water Absorption and Swelling. The water absorption and swelling behavior of nanocomposite gels are closely related to their drug release properties. To reveal the effect of bentonite modification on the release properties of SA nanocomposite gels, the water absorption kinetics of SA nanocomposite gels containing different contents of CCB were investigated. As shown in Figure 8A, water absorption and swelling of the CCB−SA gel particles were rapid processes, with all of the gel particles experiencing a rapid increase in water absorption in the initial phase followed by a slight decrease and essentially reaching saturation after 20 min. Similar shrinkage was observed at the initial stage of water absorption and swelling of Fe^{3+} cross-linked carboxymethyl-cellulose, which was related to the shell−core structure of the hydrogel prepared by the multivalent cation cross-linking method. Li et al. suggested that the concentration of metal cations in the shell layer was higher than that in the core region and that the metal ions enriched in the shell layer would diffuse toward the core region to form a thicker shell layer during water absorption and swelling, which limited the swelling of the gel due to the formation of an irreversible network structure.[56]

To further reveal the effect of CC modification on B−SA nanocomposite gels, the relative changes in water absorption of CCB−SA nanocomposite gel particles were calculated based on the saturated water absorption of SA gels and compared with the results of previous works (Figure 8B). The results indicated that the addition of equal amounts of CCB would result in lower water absorption of SA composite gels, a phenomenon that could be attributed to two factors: (1) the hydrophilicity of the bentonite nanoplatelet surface was reduced through CC modification and (2) the electrostatic interaction between the CC bound to the bentonite surface and the SA molecules not only reduced the hydrophilicity of the carboxyl groups of the SA molecules but also hindered the movement of the SA molecules and the water absorption of the gels. Also, saturation water absorption of the CCB−SA nanocomposite gels continued to decrease with increasing amounts of CCB while that of the B−SA nanocomposite gels decreased and then increased, reaching a minimum at approximately 10% of clay content, which difference mainly resulted from the stronger interaction between the bentonite nanoplatelets and the SA molecular chain due to the CC modification. The XRD and SEM analyses showed that the bentonite nanoplatelets were well dispersed in the gel via the electrostatic interaction between the CC bound on the surface and the SA molecules, and only slight aggregation of the bentonite nanoplatelets was observed even at 30% addition (Figures 5B and 6). In contrast, significant aggregation of bentonite and cracks was clearly observed on the surface of the B−SA gel film at 10% bentonite addition, which indicated a limitation of their interactions, thus increasing the porosity and water absorption of the gel particles (Figure S2).

3.9. Drug Release and Kinetic Studies. To reveal the effect of bentonite modification on the release properties of B−SA nanocomposite gels, the release kinetics of alachlor from the gel particles were determined by encapsulating alachlor in B−SA and CCB−SA nanocomposite gel particles, respectively. The release pattern of alachlor from the two nanocomposite gel particles was found to be similar; that is, the release rates first decreased and then increased as the mass percentage of clay in the nanocomposite gels increased. The cumulative release curves of alachlor from both A−B$_y$−SA and A−$CC_{10}B_y$−SA nanocomposite gel particles were presented in the paper (Figure 9), and the Rigter−Peppas empirical equation was applied to fit the alachlor release data.[57,58]
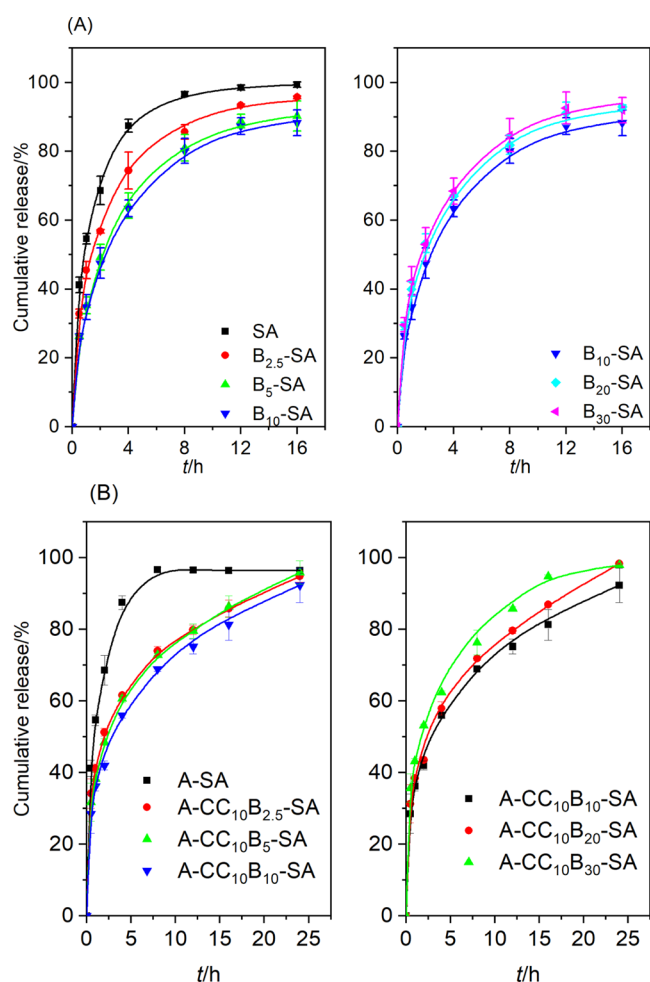
Figure 9. Release kinetics of alachlor from alginate nanocomposites with bentonite (A) and cationic cellulose-modified bentonite (B).

$$M_t/M_0 = kt^n \tag{1}$$

where M_t/M_0 is the drug release rate at moment t, k is a constant, and n is the diffusion exponent. The k and n of alachlor release were calculated by the nonlinear fitting of the release data according to the least-squares method and the release time of 50% of alachlor from the particles (T_{50}) was further calculated, and the results are shown in Table 3.

The diffusion coefficient n is the basis for the analysis of the drug release mechanism. Typically, the release of the active ingredient from a sphere release system was dominated by Fickian diffusion when the diffusion exponent $n \leq 0.43$, $0.43 < n < 0.85$ corresponding to the non-Fickian transport, and $n > 0.85$ indicating a case II transport.[59] The results in Table 3 showed that the diffusion exponent n of alachlor from clay–alginate nanocomposite gel particles ranged from 0.22 to 0.33, suggesting that the release of alachlor was mainly dominated by the Fickian diffusion. Alachlor was dispersed in the gel network in the form of molecules or microemulsion droplets and would dissolve and diffuse as the gel swelled with water uptake, eventually releasing into the medium under the effect of a concentration gradient. Therefore, the release of alachlor would be delayed by the hindering effect of the bentonite nanoparticles and SA polymer chains, which was the rate-controlling step.

The rate of diffusive release of drugs is mainly related to the adsorption capacity and permeability of the matrix. The enhanced adsorption capacity of the matrix means a lower equilibrium concentration and release rate of the drug in the release medium.[60] Comparison with previous work revealed that the adsorption capacity of bentonite for alachlor ($K_a = 140$ mL·g^{-1}) was significantly higher than that of imidacloprid ($K_a = 1.1$ mL·g^{-1}). Accordingly, the B–SA nanocomposite gel had a better sustained-release property on the former, and the release time of 50% alachlor and imidacloprid active ingredient (T_{50}) from B–SA nanocomposite gels was 4.4 and 2.5 times longer than that of release from pure SA gel. The adsorption capacity of bentonite for alachlor was significantly enhanced by the CC modification (Table 1), which was more effective in retarding the release of alachlor than the B–SA nanocomposite gels. Also, the T_{50} value of the SA nanocomposite gel containing 10% CCB was 5.6 times that of the release from the pure SA gel (Table 3).

The permeability of the matrix is another major factor in the diffusion of drug molecules. As illustrated in Figure 6, a decline in the release of alachlor over time was observed for all formulations, probably due to an increase in the distance where dissolved molecules had to diffuse as the depleted zone advanced to the center of the matrix. In diffusion-controlled matrix systems, this usually means that the release is proportional to the square root of time, and the Higuchi equation is commonly used to describe the release process of similar release systems[61]

Table 3. Simulation Parameters of the Release Curves of Alachlor from Bentonite (Modified Bentonite)–Alginate Nanocomposite Gels Using the Rigter–Peppas Model and Higuchi Model

sample	Rigter–Peppas				Higuchi		
	$k/(h^{-n})$	n	T_{50}/h	R^2	$K_H \times 10^2/h^{-1/2}$	$P \times 10^2/(h^{-1} \cdot mm^2)$	R
A–SA	57.2(3.8)	0.22(0.03)	0.54	0.965	14.3(0.3)	49.83	0.999
A–B$_{2.5}$–SA	46.4(2.2)	0.28(0.02)	1.32	0.987	11.1(0.3)	14.89	0.999
A–B$_5$–SA	38.1(2.1)	0.33(0.03)	2.26	0.987	9.0(0.1)	9.75	0.999
A–B$_{10}$–SA	37.5(2.2)	0.33(0.03)	2.37	0.986	8.9(0.1)	7.77	0.999
A–B$_{20}$–SA	41.6(1.8)	0.31(0.02)	1.82	0.991	9.1(0.4)	11.02	0.997
A–B$_{30}$–SA	42.8(2.3)	0.30(0.02)	1.68	0.986	10.0(0.4)	12.88	0.998
A–CC$_{10}$B$_{2.5}$–SA	42.3(1.5)	0.26(0.02)	1.92	0.998	6.3(0.1)	9.13	0.989
A–CC$_{10}$B$_5$–SA	39.8(1.1)	0.28(0.01)	2.28	0.999	6.2(0.2)	8.64	0.993
A–CC$_{10}$B$_{10}$–SA	35.9(2.2)	0.30(0.02)	3.05	0.998	6.1(0.2)	8.06	0.994
A–CC$_{10}$B$_{20}$–SA	37.6(0.5)	0.30(0.03)	2.57	0.999	7.0(0.3)	10.95	0.995
A–CC$_{10}$B$_{30}$–SA	43.8(1.4)	0.26(0.01)	1.66	0.996	7.3(0.3)	12.45	0.992

$$\{0.5[1 - (1 - M_t/M_0)^{2/3} - 2M_t/(3M_0)]\}^{1/2} = K_H t^{1/2} \tag{2}$$

$$K_H = [P/(C_0 r^2)]^{1/2} \tag{3}$$

where M_t/M_0 is the drug release rate at moment t and K_H is a constant related to the radius r of the particle, the starting concentration C_0 of the active ingredient, and the permeability P of the system.

K_H and P values were obtained by a nonlinear fit of the alachlor release data using eqs 2 and 3. Similar to the previous work,[25] the permeability of the B−SA nanocomposite gels to alachlor first decreased and then increased as the mass percentage of bentonite content increased, with a minimum at addition of 10%, which was mainly caused by the aggregation of bentonite nanoplatelets and the structural changes in the alginate nanocomposite gel. The CCB−SA nanocomposite gels had the same pattern of variation in permeability and had lower permeability with the same mass percentage of nanoclay contained, which benefited from the stronger interaction between the CCB and SA molecular chains, and this ultimately resulted in a better sustained-release property.

4. CONCLUSIONS

The cationic cellulose-modified bentonite−alginate nanocomposite gels were successfully prepared. The release of alachlor from the modified bentonite−alginate nanocomposite gels was mainly dominated by the Fickian diffusion and was closely related to the adsorption capacity and permeability of the nanocomposite gels. The adsorption of alachlor on bentonite was dominated by the hydrophobic interaction of the nonpolar groups of alachlor with the exposed siloxane surface on the bentonite nanoplatelets. Cationic cellulose bound with the negative charge sites on the surface of the bentonite nanoplatelets through an ion exchange reaction, which not only enhanced the hydrophobicity of the bentonite surface and its interaction with alachlor but also the modified bentonite formed a tighter structure through the electrostatic interaction between cationic cellulose and alginate molecular chains, effectively reducing the stacking and aggregation of the bentonite nanoplatelets and reducing the water absorption and swelling and permeability of the alginate gel. Compared with bentonite, the alginate gel obtained better sustained-release properties by adding cationic cellulose-modified bentonite. The release rate of alachlor first decreased and then increased with the addition of bentonite and modified bentonite to the nanocomposite gel and was most effective in delaying the release of alachlor at addition of about 10%. Under these conditions, the release time of 50% alachlor from bentonite−alginate and modified bentonite−alginate nanocomposite gels was 4.4 and 5.6 times longer than that of the release from the pure alginate gel, respectively. These features triggered the cationic cellulose-modified bentonite−alginate nanocomposite gel to serve as a promising sustained-release carrier for pesticides.

■ ASSOCIATED CONTENT

Ⓢⓘ Supporting Information

The Supporting Information is available free of charge at https://pubs.acs.org/doi/10.1021/acsomega.2c01805.

Figure S1, release kinetics of alachlor from alginate nanocomposites with organobentonite modified with cationic cellulose of different loading levels; Figure S2, SEM images of alachlor-loaded bentonite−alginate nanocomposites; and Table S1, dehydration mass loss rate and the initial mass loss temperature of bentonite, cationic cellulose, and cationic cellulose-modified bentonite (PDF)

■ AUTHOR INFORMATION

Corresponding Author

Lin Ma − *School of Chemistry and Chemical Engineering, Guangxi University, Nanning 530004, P. R. China;* ⓞ orcid.org/0000-0001-9061-1080; Email: malinzju@163.com

Authors

Xiaocheng Wang − *School of Chemistry and Chemical Engineering, Guangxi University, Nanning 530004, P. R. China;* ⓞ orcid.org/0000-0002-1694-866X

Xiaojun Hou − *School of Chemistry and Chemical Engineering, Guangxi University, Nanning 530004, P. R. China*

Peiyu Zou − *School of Chemistry and Chemical Engineering, Guangxi University, Nanning 530004, P. R. China*

Min Zhang − *School of Chemistry and Chemical Engineering, Guangxi University, Nanning 530004, P. R. China*

Complete contact information is available at:
https://pubs.acs.org/10.1021/acsomega.2c01805

Author Contributions

X.W.: conceptualization, methodology, validation, and writing—original draft. X.H.: investigation and formal analysis. P.Z.: investigation and formal analysis. M.Z.: supervision, investigation, and formal analysis. L.M.: conceptualization, supervision, project administration, funding acquisition, and writing—review and editing.

Notes

The authors declare no competing financial interest.

■ ACKNOWLEDGMENTS

■ REFERENCES

(1) Leong, W. H.; Teh, S. Y.; Hossain, M. M.; Nadarajaw, T.; Zabidi-Hussin, Z.; Chin, S. Y.; Lai, K. S.; Lim, S. E. Application, monitoring and adverse effects in pesticide use: The importance of reinforcement of Good Agricultural Practices (GAPs). *J. Environ. Manage.* **2020**, *260*, No. 109987.

(2) Musarurwa, H.; Tavengwa, N. T. Emerging green solvents and their applications during pesticide analysis in food and environmental samples. *Talanta* **2021**, *223*, No. 121507.

(3) Tudi, M.; Daniel Ruan, H.; Wang, L.; Lyu, J.; Sadler, R.; Connell, D.; Chu, C.; Phung, D. T. Agriculture Development, Pesticide Application and Its Impact on the Environment. *Int. J. Environ. Res. Public Health* **2021**, *18*, No. 1112.

(4) Chariou, P. L.; Dogan, A. B.; Welsh, A. G.; Saidel, G. M.; Baskaran, H.; Steinmetz, N. F. Soil mobility of synthetic and virus-based model nanopesticides. *Nat Nanotechnol.* **2019**, *14*, 712−718.

(5) Volova, T.; Prudnikova, S.; Boyandin, A.; Zhila, N.; Kiselev, E.; Shumilova, A.; Baranovskiy, S.; Demidenko, A.; Shishatskaya, E.; Thomas, S. Constructing Slow-Release Fungicide Formulations Based on Poly(3-hydroxybutyrate) and Natural Materials as a Degradable Matrix. *J. Agric. Food Chem.* **2019**, *67*, 9220−9231.

(6) Zhao, M.; Zhou, H.; Chen, L.; Hao, L.; Chen, H.; Zhou, X. Carboxymethyl chitosan grafted trisiloxane surfactant nanoparticles with pH sensitivity for sustained release of pesticide. *Carbohydr. Polym.* **2020**, *243*, No. 116433.

(7) Li, M.; Li, H.; Li, X.; Zhu, H.; Xu, Z.; Liu, L.; Ma, J.; Zhang, M.; Bioinspired, A. Alginate-Gum Arabic Hydrogel with Micro-/Nano-scale Structures for Controlled Drug Release in Chronic Wound Healing. *ACS Appl. Mater. Interfaces* **2017**, *9*, 22160−22175.

(8) George, D.; Maheswari, P. U.; Begum, K. Synergic formulation of onion peel quercetin loaded chitosan-cellulose hydrogel with green zinc oxide nanoparticles towards controlled release, biocompatibility, antimicrobial and anticancer activity. *Int. J. Biol. Macromol.* **2019**, *132*, 784−794.

(9) Xu, X.; Gu, Z.; Chen, X.; Shi, C.; Liu, C.; Liu, M.; Wang, L.; Sun, M.; Zhang, K.; Liu, Q.; Shen, Y.; Lin, C.; Yang, B.; Sun, H. An injectable and thermosensitive hydrogel: Promoting periodontal regeneration by controlled-release of aspirin and erythropoietin. *Acta Biomater.* **2019**, *86*, 235−246.

(10) Martínez-Gómez, F.; Guerrero, J.; Matsuhiro, B.; Pavez, J. In vitro release of metformin hydrochloride from sodium alginate/polyvinyl alcohol hydrogels. *Carbohydr. Polym.* **2017**, *155*, 182−191.

(11) Mahanta, A. K.; Senapati, S.; Paliwal, P.; Krishnamurthy, S.; Hemalatha, S.; Maiti, P. Nanoparticle-Induced Controlled Drug Delivery Using Chitosan-Based Hydrogel and Scaffold: Application to Bone Regeneration. *Mol. Pharm.* **2019**, *16*, 327−338.

(12) Xu, Q.; Huang, W.; Jiang, L.; Lei, Z.; Li, X.; Deng, H. KGM and PMAA based pH-sensitive interpenetrating polymer network hydrogel for controlled drug release. *Carbohydr Polym.* **2013**, *97*, 565−570.

(13) Stenger, M.; Klein, K.; Gronnemose, R. B.; Klitgaard, J. K.; Kolmos, H. J.; Lindholt, J. S.; Alm, M.; Thomsen, P.; Andersen, T. E. Co-release of dicloxacillin and thioridazine from catheter material containing an interpenetrating polymer network for inhibiting device-associated Staphylococcus aureus infection. *J. Controlled Release* **2016**, *241*, 125−134.

(14) Boyer, C.; Figueiredo, L.; Pace, R.; Lesoeur, J.; Rouillon, T.; Visage, C. L.; Tassin, J. F.; Weiss, P.; Guicheux, J.; Rethore, G. Laponite nanoparticle-associated silated hydroxypropylmethyl cellulose as an injectable reinforced interpenetrating network hydrogel for cartilage tissue engineering. *Acta Biomater.* **2018**, *65*, 112−122.

(15) He, X.; Deng, H.; Hwang, H. M. The current application of nanotechnology in food and agriculture. *J. Food Drug Anal.* **2019**, *27*, 1−21.

(16) Kumar, S.; Nehra, M.; Dilbaghi, N.; Marrazza, G.; Hassan, A. A.; Kim, K. H. Nano-based smart pesticide formulations: Emerging opportunities for agriculture. *J. Controlled Release* **2019**, *294*, 131−153.

(17) Sarkar, D. J.; Singh, A. Base triggered release of insecticide from bentonite reinforced citric acid crosslinked carboxymethyl cellulose hydrogel composites. *Carbohydr. Polym.* **2017**, *156*, 303−311.

(18) He, F.; Zhou, Q.; Wang, L.; Yu, G.; Li, J.; Feng, Y. Fabrication of a sustained release delivery system for pesticides using inter-penetrating polyacrylamide/alginate/montmorillonite nanocomposite hydrogels. *Appl. Clay Sci.* **2019**, *183*, No. 105347.

(19) Wang, L.; Yu, G.; Li, J.; Feng, Y.; Peng, Y.; Zhao, X.; Tang, Y.; Zhang, Q. Stretchable hydrophobic modified alginate double-network nanocomposite hydrogels for sustained release of water-insoluble pesticides. *J. Cleaner Prod.* **2019**, *226*, 122−132.

(20) Mahmood, A.; Sharif, A.; Muhammad, F.; Sarfraz, R. M.; Abrar, M. A.; Qaisar, M. N.; Anwar, N.; Amjad, M. W.; Zaman, M. Development and in vitro evaluation of (β-cyclodextrin-g-methacrylic acid)/Na+-montmorillonite nanocomposite hydrogels for controlled delivery of lovastatin. *Int. J. Nanomed.* **2019**, *14*, 5397−5413.

(21) Shen, Y.; Jiao, S.; Ma, Z.; Lin, H.; Gao, W.; Chen, J. Humic acid-modified bentonite composite material enhances urea-nitrogen use efficiency. *Chemosphere* **2020**, *255*, No. 126976.

(22) Jafari, H.; Atlasi, Z.; Mahdavinia, G. R.; Hadifar, S.; Sabzi, M. Magnetic kappa-carrageenan/chitosan/montmorillonite nanocomposite hydrogels with controlled sunitinib release. *Mater. Sci. Eng., C* **2021**, *124*, No. 112042.

(23) Lisuzzo, L.; Giuseppe, C.; Stefana, M.; Giuseppe, L. Layered composite based on halloysite and natural polymers: a carrier for the pH controlled release of drugs. *New J. Chem.* **2019**, *43*, 10887.

(24) Cavallaro, G.; Lorenzo, L.; Giuseppe, L.; Stefana, M. Printable Hydrogels Based on Alginate and Halloysite Nanotubes. *Int. J. Mol. Sci.* **2022**, *23*, 3294.

(25) Zhang, H.; Shi, Y.; Xu, X.; Zhang, M.; Ma, L. Structure Regulation of Bentonite-Alginate Nanocomposites for Controlled Release of Imidacloprid. *ACS Omega* **2020**, *5*, 10068−10076.

(26) Jesus, C. R. N.; Molina, E. F.; Pulcinelli, S. H.; Santilli, C. V. Highly Controlled Diffusion Drug Release from Ureasil-Poly(ethylene oxide)-Na(+)-Montmorillonite Hybrid Hydrogel Nanocomposites. *ACS Appl. Mater. Interfaces* **2018**, *10*, 19059−19068.

(27) Bhardwaj, D.; Sharma, M.; Sharma, P.; Tomar, R. Synthesis and surfactant modification of clinoptilolite and montmorillonite for the removal of nitrate and preparation of slow release nitrogen fertilizer. *J. Hazard Mater.* **2012**, *227−228*, 292−300.

(28) Zhu, X.; Wen, Y.; Cheng, D.; Li, C.; An, X.; Ni, Y. Cationic amphiphilic microfibrillated cellulose (MFC) for potential use for bile acid sorption. *Carbohydr. Polym.* **2015**, *132*, 598−605.

(29) Zhao, S.; Cheng, F.; Chen, Y.; Wei, Y. The interactions between cationic cellulose and Gemini surfactant in aqueous solution. *Carbohydr. Polym.* **2016**, *141*, 68−74.

(30) Oprea, M.; Voicu, S. I. Recent advances in composites based on cellulose derivatives for biomedical applications. *Carbohydr. Polym.* **2020**, *247*, No. 116683.

(31) Hokkanen, S.; Bhatnagar, A.; Sillanpaa, M. A review on modification methods to cellulose-based adsorbents to improve adsorption capacity. *Water Res.* **2016**, *91*, 156−173.

(32) Zhang, F.; Pang, Z.; Dong, C.; Liu, Z. Preparing cationic cotton linter cellulose with high substitution degree by ultrasonic treatment. *Carbohydr. Polym.* **2015**, *132*, 214−220.

(33) Kono, H.; Ogasawara, K.; Kusumoto, R.; Oshima, K.; Hashimoto, H.; Shimizu, Y. Cationic cellulose hydrogels cross-linked by poly(ethylene glycol): Preparation, molecular dynamics, and adsorption of anionic dyes. *Carbohydr. Polym.* **2016**, *152*, 170−180.

(34) Ejaz, U.; Muhammad, S.; Ali, F. I.; Hashmi, I. A.; Sohail, M. Cellulose extraction from methyltrioctylammonium chloride pre-treated sugarcane bagasse and its application. *Int. J. Biol. Macromol.* **2020**, *165*, 11−17.

(35) Zaman, M.; Xiao, H.; Chibante, F.; Ni, Y. Synthesis and characterization of cationically modified nanocrystalline cellulose. *Carbohydr. Polym.* **2012**, *89*, 163−170.

(36) He, Y.; Wu, Z.; Tu, L.; Han, Y.; Zhang, G.; Li, C. Encapsulation and characterization of slow-release microbial fertilizer from the composites of bentonite and alginate. *Appl. Clay Sci.* **2015**, *109−110*, 68−75.

(37) Huang, C.; Fang, G.; Tao, Y.; Meng, X.; Lin, Y.; Bhagia, S.; Wu, X.; Yong, Q.; Ragauskas, A. J. Nacre-inspired hemicelluloses paper with fire retardant and gas barrier properties by self-assembly with bentonite nanosheets. *Carbohydr. Polym.* **2019**, *225*, No. 115219.

(38) Tao, Y.; Huang, C.; Lai, C.; Huang, C.; Yong, Q. Biomimetic galactomannan/bentonite/graphene oxide film with superior mechanical and fire retardant properties by borate cross-linking. *Carbohydr. Polym.* **2020**, *245*, No. 116508.

(39) Liu, H.; Liu, D.; Yao, F.; Wu, Q. Fabrication and properties of transparent polymethylmethacrylate/cellulose nanocrystals composites. *Bioresour. Technol.* **2010**, *101*, 5685−5692.

(40) Caglar, B.; Afsin, B.; Tabak, A.; Eren, E. Characterization of the cation-exchanged bentonites by XRPD, ATR, DTA/TG analyses and BET measurement. *Chem. Eng. J.* **2009**, *149*, 242−248.

(41) Almonaityte, K.; Bendoraitiene, J.; Babelyte, M.; Rosliuk, D.; Rutkaite, R. Structure and properties of cationic starches synthesized by using 3-chloro-2-hydroxypropyltrimethylammonium chloride. *Int. J. Biol. Macromol.* **2020**, *164*, 2010−2017.

(42) Vaezi, K.; Asadpour, G.; Sharifi, S. H. Bio nanocomposites based on cationic starch reinforced with montmorillonite and cellulose nanocrystals: Fundamental properties and biodegradability study. *Int. J. Biol. Macromol.* **2020**, *146*, 374−386.

(43) Ma, J.; Khan, M. A.; Xia, M.; Fu, C.; Zhu, S.; Chu, Y.; Lei, W.; Wang, F. Effective adsorption of heavy metal ions by sodium lignosulfonate reformed montmorillonite. *Int. J. Biol Macromol.* **2019**, *138*, 188−197.

(44) Abbasi, A. R.; Sohail, M.; Minhas, M. U.; Khaliq, T.; Kousar, M.; Khan, S.; Hussain, Z.; Munir, A. Bioinspired sodium alginate based thermosensitive hydrogel membranes for accelerated wound healing. *Int. J. Biol. Macromol.* **2020**, *155*, 751−765.

(45) Asgari, M.; Abouelmagd, A.; Sundararaj, U. Silane functionalization of sodium montmorillonite nanoclay and its effect on rheological and mechanical properties of HDPE/clay nanocomposites. *Appl. Clay Sci.* **2017**, *146*, 439−448.

(46) Parikh, A.; Madamwar, D. Partial characterization of extracellular polysaccharides from cyanobacteria. *Bioresour. Technol.* **2006**, *97*, 1822−1827.

(47) Gabryś, T.; Fryczkowska, B.; Binias, D.; Slusarczyk, C.; Fabia, J. Preparation and properties of composite cellulose fibres with the addition of graphene oxide. *Carbohydr. Polym.* **2021**, *254*, No. 117436.

(48) Zhang, X.; Li, Y.; Hou, Y. Preparation of magnetic polyethylenimine lignin and its adsorption of Pb(II). *Int. J. Biol. Macromol.* **2019**, *141*, 1102−1110.

(49) Liu, Z.; Chen, M.; Guo, Y.; Wang, X.; Zhang, L.; Zhou, J.; Li, H.; Shi, Q. Self-assembly of cationic amphiphilic cellulose-g-poly (p-dioxanone) copolymers. *Carbohydr Polym.* **2019**, *204*, 214−222.

(50) Godiya, C. B.; Liang, M.; Sayed, S. M.; Li, D.; Lu, X. Novel alginate/polyethyleneimine hydrogel adsorbent for cascaded removal and utilization of Cu2+ and Pb2+ ions. *J. Environ. Manage.* **2019**, *232*, 829−841.

(51) Sapalidis, A. A.; Katsaros, F. K.; Steriotis, T. A.; Kanellopoulos, N. K. Properties of poly(vinyl alcohol)-Bentonite clay nanocomposite films in relation to polymer-clay interactions. *J. Appl. Polym. Sci.* **2012**, *123*, 1812−1821.

(52) Wang, Y.; Xiong, Y.; Wang, J.; Zhang, X. Ultrasonic-assisted fabrication of montmorillonite-lignin hybrid hydrogel: Highly efficient swelling behaviors and super-sorbent for dye removal from wastewater. *Colloids Surf., A* **2017**, *520*, 903−913.

(53) Bharadwaj, R.; Mehrabia, A. R.; Hamiltona, C.; Trujilloa, C.; Murgaa, M.; Fana, R.; Chaviraa, A.; Thompsonb, A. K. Structure−property relationships in cross-linked polyester−clay nanocomposites. *Polymer* **2002**, *43*, 3699−3705.

(54) Chang, J.-H.; An, Y. U.; Cho, D.; Giannelis, E. P. Poly(lactic acid) nanocomposites: comparison of their properties with montmorillonite and synthetic mica (II). *Polymer* **2003**, *44*, 3715−3720.

(55) Giroto, A. S.; de Campos, A.; Pereira, E. I.; Cruz, C. C. T.; Marconcini, J. M.; Ribeiro, C. Study of a nanocomposite starch-clay for slow-release of herbicides: Evidence of synergistic effects between the biodegradable matrix and exfoliated clay on herbicide release control. *J. Appl. Polym. Sci.* **2014**, *131*, 41188−41197.

(56) Li, J.; Lu, J.; Li, Y. Carboxylmethylcellulose/bentonite composite gels: Water sorption behavior and controlled release of herbicide. *J. Appl. Polym. Sci.* **2009**, *112*, 261−268.

(57) Colombo, P.; Bettini, R.; Santi, P.; Ascentiis, A. D.; Peppas, N. A. Analysis of the swelling and release mechanisms from drug delivery systems with emphasis on drug solubility and water transport. *J. Controlled Release* **1996**, *39*, 231−237.

(58) Ritger, P. L.; Peppas, N. A. A simple equation for description of solute release II: Fickian and anomalous release from swellable devices. *J. Controlled Release* **1987**, *5*, 37−42.

(59) Budinčić, J. M.; Petrovic, L.; Dekic, L.; Fraj, J.; Bucko, S.; Katona, J.; Spasojevic, L. Study of vitamin E microencapsulation and controlled release from chitosan/sodium lauryl ether sulfate microcapsules. *Carbohydr. Polym.* **2021**, *251*, No. 116988.

(60) Fernández-Pérez, M.; Villafranca-Sánchez, M.; Flores-Céspedes, F.; Garrido-Herrera, F. J.; Pérez-García, S. Use of bentonite and activated carbon in controlled release formulations of carbofuran. *J. Agric. Food Chem.* **2005**, *53*, 6697−6703.

(61) Higuchi, T. Mechanism of sustained-action medication. Theoretical analysis of rate of release of solid drugs dispersed in solid matrices. *J. Pharm. Sci.* **1963**, *52*, 1145−1149.